energy&fuels

pubs.acs.org/EF
Article

Mechanochemically Engineered CaO−CeO_2 Dual-Function Catalysts for Sustainable Glycerol Carbonate Production without Solvents

Published as part of Energy & Fuels special issue "Celebrating Authors of Energy and Fuels Most-Impactful Articles (2022)".

Patcharaporn Inrirai, Runzhe Yu, Daniel Goma Jiménez, Nancy Artioli, and Haresh Manyar*

Cite This: https://doi.org/10.1021/acs.energyfuels.5c01580

ABSTRACT: Upgrading biorefinery-derived waste such as glycerol to fuel-additives and high-value products is essential to further enhance the productivity, profitability, and circularity of the biorefinery concept to achieve a green and sustainable net-zero world. This study explores the catalytic conversion of glycerol into glycerol carbonate using calcium oxide−cerium oxide (CaO−CeO_2) dual-function catalytic materials. Herein, a clean and efficient approach was developed to synthesize CaO−CeO_2 materials using a green mechanochemical method and then utilize these as catalyst in sustainable and solvent-free synthesis of glycerol carbonate to enhance the circular economy of biorefineries while reducing their carbon footprint. The catalysts were comprehensively characterized using XRD, FTIR, ICP, N_2 sorption, CO_2-TPD, and SEM/EDS analyses and evaluated for their catalytic activity. Among the catalysts studied, 40 wt % CaO−CeO_2 exhibited the highest catalytic activity, achieving 95% glycerol conversion and 99% selectivity to glycerol carbonate under optimized conditions (10 wt % catalyst loading relative to glycerol, 90 °C, 60 min, and a glycerol/ DMC molar ratio of 1:3). This catalyst showed excellent reusability, maintaining high conversion over four cycles. The transesterification reaction followed irreversible second-order reaction kinetics with an activation energy of 46.9 kJ mol^{-1}. The synergistic interplay between the basic sites of the Ca^{2+}−O^{2-} pair and the oxygen vacancies in the CeO_2 matrix at the CaO−CeO_2 interface work in tandem to enhance the catalytic activity for glycerol carbonate production. We have developed a highly efficient, cost-effective, and environment-friendly approach for the sustainable production of glycerol carbonate from glycerol.

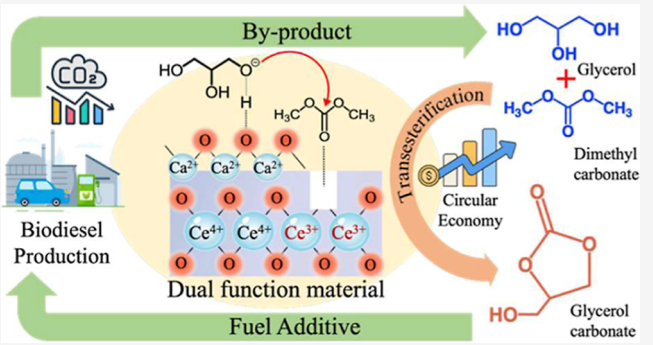

1. INTRODUCTION

The increasing global demand for energy has intensified environmental challenges, particularly due to greenhouse gas emissions, with carbon dioxide (CO_2) being a major contributor. Biodiesel is widely recognized as a sustainable alternative to fossil fuels, offering significant reductions in CO_2, carbon monoxide (CO), sulfur oxides (SO_x), particulate matter (PM), and volatile organic compounds (VOCs) emissions.[1]

Global biodiesel production has doubled from 20 million tons in 2010 to 40 million tons in 2022, with projections indicating stable production levels in the near future.[2,3] However, the biodiesel industry generates glycerol as a major byproduct, accounting for approximately 10% of the total production by weight. Although often considered waste, glycerol has substantial potential for value-added applications across various industries, including fuel additives, polymer synthesis, hydrogen production, fuel cells, and pharmaceuticals. Our research group has keen interest in upgrading glycerol into high-value products for advancing circular economy.[4−8] One of the promising strategies for glycerol valorization is its conversion to glycerol carbonate via transesterification. Glycerol carbonate is regarded as an excellent fuel additive due to the capability to increase the fuel octane number and oxidation stability and diminish particle emissions. By upgrading glycerol to glycerol carbonate, we can not only minimize the carbon footprint of biorefineries but also improve the economic profitability as the selling price of crude glycerol is US$210 to $390/t, while that of glycerol carbonate is around US$3000/ton. Glycerol carbonate exhibits excellent physico-

Received: March 31, 2025
Revised: May 30, 2025
Accepted: June 16, 2025

chemical properties, such as a low freezing point (−69 °C), high boiling point (137−140 °C), high density (1.4 g mL^{-1} at 25 °C), and a high dielectric constant (115).[9] Additionally, it is nontoxic, highly soluble in water, and biocompatible. Owing to its carbonyl and hydroxyl functional groups, glycerol carbonate has diverse applications, particularly as a high-value chemical intermediate for polymer production, as well as in solvents, surfactants, lubricants, cosmetics, and fuel additives.[7]

Existing research on glycerol transesterification has predominantly focused on homogeneous catalytic systems. However, homogeneous catalysts present challenges related to catalyst cost, postreaction separation, and complex product purification. To overcome these issues, heterogeneous catalysts have been explored as viable alternatives. Calcium oxide (CaO) was first introduced as a catalyst for glycerol transesterification with dimethyl carbonate by Ochoa-Gómez et al.,[10] who compared its catalytic performance with other basic materials such as magnesium oxide (MgO) and calcium carbonate ($CaCO_3$). The catalytic efficiency of CaO was significantly influenced by calcination temperature, achieving a 91% glycerol carbonate yield under optimized conditions. Similarly, Simanjuntak et al.[11] reported a CaO-catalyzed process with a 94% conversion and high selectivity to glycerol carbonate. However, catalyst deactivation occurred due to the formation of calcium glycerate complexes. To enhance the stability and reusability of CaO, researchers have explored its incorporation into supports, such as activated alumina. Lu et al.[12] demonstrated that CaO supported on activated alumina extrudates, synthesized using polyacrylamide as a pore-forming agent, exhibited superior stability compared to unsupported CaO, with the yield decreasing from 91% to 63% after six reaction cycles. Modifying CaO with basic dopants has been shown to improve both its activity and stability. For instance, doping CaO with potassium nitrate has been shown to enhance catalytic performance compared to pure CaO.[13] As a result, the development of efficient and stable catalysts remains a key research focus for the transesterification of glycerol to glycerol carbonate.

While cerium oxide (CeO_2) is generally not considered highly active in transesterification reactions, it has been identified as a beneficial component for enhancing the basicity of solid base catalysts.[14] Parameswaram et al.[15] reported that CeO_2 exhibits remarkable catalytic performance when modified with other metal oxides, leading to improved stability. Similarly, Niu et al.[16] found that introducing cerium into CaO/MgO catalysts enhances their stability by preventing the leaching of active CaO species into the reaction medium, thereby improving catalyst reusability.[17] CeO_2, a fluorite-type material, possesses oxygen vacancy defects and an inherent oxygen storage capacity (OSC),[18] both of which contribute to its catalytic efficiency. The ability of Ce cations to transition between Ce^{3+} and Ce^{4+} states facilitates electronic conductivity and lattice expansion. These unique properties make CeO_2 an effective promoter and support material in various catalytic applications.[19]

Beyond catalytic performance, factors such as separation efficiency, environmental impact, and cost-effectiveness play significant roles in catalyst development. A key advantage of CaO is its derivation from abundant and renewable natural sources, often from waste materials, aligning with the principles of a circular economy.[20,21] In this study, CaO−CeO_2 composites synthesized through greener mechanochemical methods have gained considerable attention. By optimizing the morphology and electronic properties of CaO−CeO_2, the interaction between these two components can be fine-tuned to enhance oxygen vacancy formation, thereby promoting the catalytic reaction via sorption-enhanced catalysis. Moreover, CaO−CeO_2 materials provide a cost-effective and scalable solution, making them highly attractive for industrial applications.

2. EXPERIMENTAL SECTION

2.1. Materials. All chemicals were acquired from reputable manufacturers and used without further purification. Cerium(IV) oxide (CeO_2, 99.95%) and ethanol (C_2H_5OH, >99.8%) were purchased from Sigma-Aldrich. Glycerol ($HOCH_2CH(OH)CH_2OH$, >99%), dimethyl carbonate ($C_3H_6O_3$, 99%), *p*-xylene (C_8H_{10}, 99%), and calcium oxide (CaO, 99.9%) were obtained from Alfa Aesar.

2.2. Catalyst Preparation. Supported calcium oxide (CaO) catalysts were prepared using a green mechanochemical method using cogrinding.[4,22] The required amount of CaO was mixed with CeO_2 and ground for 15 min. The resulting catalyst was then sieved using a 125 μm mesh and dried at 80 °C overnight.

2.3. Catalyst Characterization. The prepared catalysts were characterized using N_2 physisorption, elemental analysis, X-ray diffraction (XRD), Fourier-transform infrared spectroscopy (FTIR), thermogravimetric analysis (TGA), CO_2-temperature-programmed desorption (CO_2-TPD), scanning electron microscopy (SEM), and energy-dispersive X-ray spectroscopy (EDX). Surface area and porosity were analyzed using N_2 adsorption/desorption, with the surface area calculated by the Brunauer−Emmett−Teller (BET) method, while the pore volume and pore diameter were determined using the Barrett−Joyner−Halenda (BJH) method. Metal loadings of the catalysts were measured by inductively coupled plasma optical emission spectrometry (ICP-OES) by using a PerkinElmer Optima 4300 instrument. XRD patterns were recorded by using Cu Kα radiation (λ = 0.15418 nm) on a Panalytical instrument equipped with reflection geometry. The scattered intensities were collected over a wide-angle range of 5° to 80° (2θ) with a step size of 0.02°. FTIR spectra were obtained using an Agilent Technologies Cary 630 FTIR spectrometer in the 4000−450 cm^{-1} range with an ATR sampling module. TGA profiles were recorded using a Q5000 thermogravimetric analyzer (TA Instruments) to study the decomposition behavior of the catalysts under airflow conditions, with a temperature ramp of 10 °C min^{-1} to 900 °C. The basicity of the prepared catalysts was determined using CO_2-TPD analysis. The CO_2-TPD measurements were carried out on a Micromeritics MicroActive AutoChem II 2920 system, using approximately 0.2 g of catalyst powder. The catalyst samples were first heated under a helium flow to 500 °C at a rate of 10 °C min^{-1} for 60 min. After cooling to 50 °C, a 2% CO_2 in helium mixture was passed over the sample. The sample was then heated from 50 to 950 °C at a rate of 10 °C min^{-1} under helium flow. SEM images were recorded using an FEI Quanta FEG Environmental SEM to examine the catalyst morphology. In addition to imaging, EDX mapping was conducted. The EDX analysis was performed on a relatively even surface of a catalyst particle to determine the average surface density of the corresponding metal atoms.

2.4. Reaction Procedure and Analysis Method. Catalytic activity tests were performed in a 100 mL glass reactor equipped with a magnetic stirring bar and a condenser. The reactor was mechanically agitated and maintained in an isothermal oil bath at the desired temperature. In a typical reaction, glycerol (GLY), dimethyl carbonate (DMC), and the catalyst were added to the glass reactor and stirred at 800 rpm for 1 h.[4] The reaction analysis was carried out using a Clarus 500 PerkinElmer gas chromatograph equipped with a Zebron ZB-Wax column and *p*-xylene as an internal standard. For reusability studies, the catalysts were separated from the reaction mixture by centrifugation, washed with ethanol, dried overnight at 80 °C, and then calcined at 800 °C for 3 h.[20]

Glycerol conversion was calculated according to eq 1, where N_{A0} and N_{At} represent the initial moles of glycerol and the moles at a given time *t*, respectively.

https://doi.org/10.1021/acs.energyfuels.5c01580
Energy Fuels XXXX, XXX, XXX−XXX

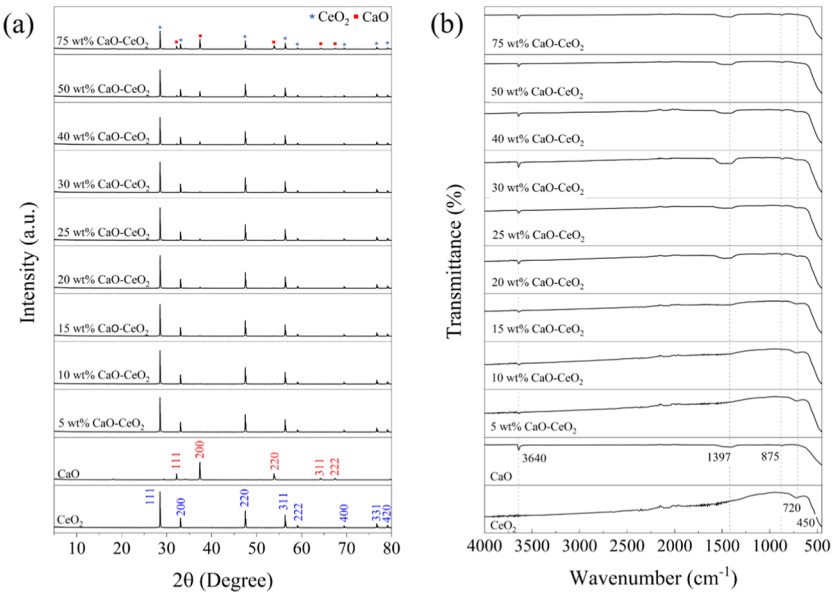

Figure 1. (a) X-ray diffraction patterns of CeO_2, CaO, and 5−75 wt % of CaO−CeO_2 catalysts, and (b) FTIR spectra of CeO_2, CaO, and 5−75 wt % of CaO−CeO_2 catalysts.

$$\text{Conversion (\%)} = \left(\frac{N_{A0} - N_{At}}{N_{A0}}\right) \times 100 \quad (1)$$

Furthermore, the selectivity of the desired product was calculated using eq 2, where A_d represents the area under the curve for the desired product and the sum A_i considers the total area of all products formed in the reaction.

$$\text{Selectivity (\%)} = \left(\frac{A_d}{A_i}\right) \times 100 \quad (2)$$

3. RESULTS AND DISCUSSION

3.1. Catalyst Characterization. The XRD patterns of the prepared catalysts are shown in Figure 1a. The diffraction peaks observed at 2θ values of 28.3°, 33.1°, 47.4°, 56.2°, 59.2°, 69.5°, 76.6°, and 79.0° correspond to the (111), (200), (220), (311), and (222) planes of the pure fluorite cubic structure of CeO_2.[23] The characteristic diffraction peaks corresponding to CaO are (111), (200), (220), (311), (222), and (400).[23] The incorporation of CaO into the CeO_2 matrix resulted in negligible changes to the XRD patterns of CeO_2. The CaO phase exhibited relatively low-intensity peaks, while strong reflections corresponding to the fluorite-type cubic structure of CeO_2 were identified in the XRD pattern.[24] Upon doping 15 wt % CaO onto CeO_2, additional diffraction peaks of CaO emerged at 2θ values of 23° and 37°, with their intensity increasing as the CaO content in the catalyst increased.

The FTIR spectra of CaO, CeO_2, and CaO−CeO_2 catalysts are shown in Figure 1b. All spectra exhibit a broad absorption band around 450 cm^{-1}, attributed to Ca−O, Ce−O, and Ca−O−Ce stretching vibrations.[24] The peak at 875 cm^{-1} corresponds to the out-of-plane stretching vibrations of the carbonate group (CO_3). The band at 1397 cm^{-1} is characteristic of asymmetric C−O stretching in the carbonate group. The two bands around 1571 cm^{-1} can be assigned to different C−H vibrational modes. The band observed around 3640 cm^{-1} corresponds to the stretching of hydroxyl groups from hydroxide species.[23,25]

The total basicity of the prepared catalysts was evaluated using temperature-programmed desorption of CO_2, with the quantified basicity values presented in Table 1. Pure CaO exhibited a basicity of 0.577 mmol g^{-1}, whereas pure CeO_2 showed no detectable basic sites on its surface. However, upon doping CeO_2 with CaO, the basicity of the catalysts increased progressively from 0.131 mmol g^{-1} to 0.540 mmol g^{-1}, as the CaO content increased from 5 to 40 wt %. When the CaO content exceeded 50 wt % in the prepared catalysts, the total basicity continued to increase, surpassing that of pure CaO. A basicity of 0.739 mmol g^{-1} was observed for the 75 wt % CaO−CeO_2 catalyst, which could be attributed to the synergistic interaction between CaO and CeO_2.[26] The TPD-CO_2 profiles of pure CeO_2, CaO, and CaO-doped CeO_2

Table 1. BET Surface Area, Pore Volume, Average Pore Diameter, and Total Basicity of the Prepared Catalysts

catalyst	BET surface area (m^2 g^{-1})	pore volume (cm^3 g^{-1})	average pore diameter (nm)	total basicity (mmol g^{-1})
CeO_2	2.46	0.0063	11.78	0.000
5 wt % CaO−CeO_2	2.71	0.0074	12.53	0.131
10 wt % CaO−CeO_2	2.28	0.0071	19.41	0.135
15 wt % CaO−CeO_2	2.35	0.0075	13.52	0.234
20 wt % CaO−CeO_2	2.00	0.0067	20.34	0.245
25 wt % CaO−CeO_2	2.18	0.0079	18.46	0.335
30 wt % CaO−CeO_2	2.80	0.0110	18.30	0.452
40 wt % CaO−CeO_2	2.50	0.0092	15.23	0.540
50 wt % CaO−CeO_2	3.25	0.0132	16.72	0.593
75 wt % CaO−CeO_2	3.15	0.0142	18.56	0.739
CaO	1.80	0.0085	21.80	0.577

https://doi.org/10.1021/acs.energyfuels.5c01580
Energy Fuels XXXX, XXX, XXX−XXX

catalysts are presented in Figure 2, showing desorption behavior from 100 to 800 °C. Desorption peaks below 200 °C indicate the presence of weak basic sites, while peaks in the 200−570 °C range are related to moderate basic sites. The peaks at high temperatures correspond to the strong basic sites.[27] Pure CeO_2 showed no detectable basic sites on its surface, whereas the CaO catalyst exhibited both moderate and strong basic sites. With 5−10 wt % CaO incorporated into CeO_2, moderate basic sites were observed. As the CaO content increased, the enhanced basicity of the prepared catalysts led to a shift toward strong basic sites. 50 and 75 wt % CaO−CeO_2 catalysts exhibited a higher density of strong basic sites compared to pure CaO. The total basicity values of all catalysts, shown in Table 1, align well with the TCD signals.

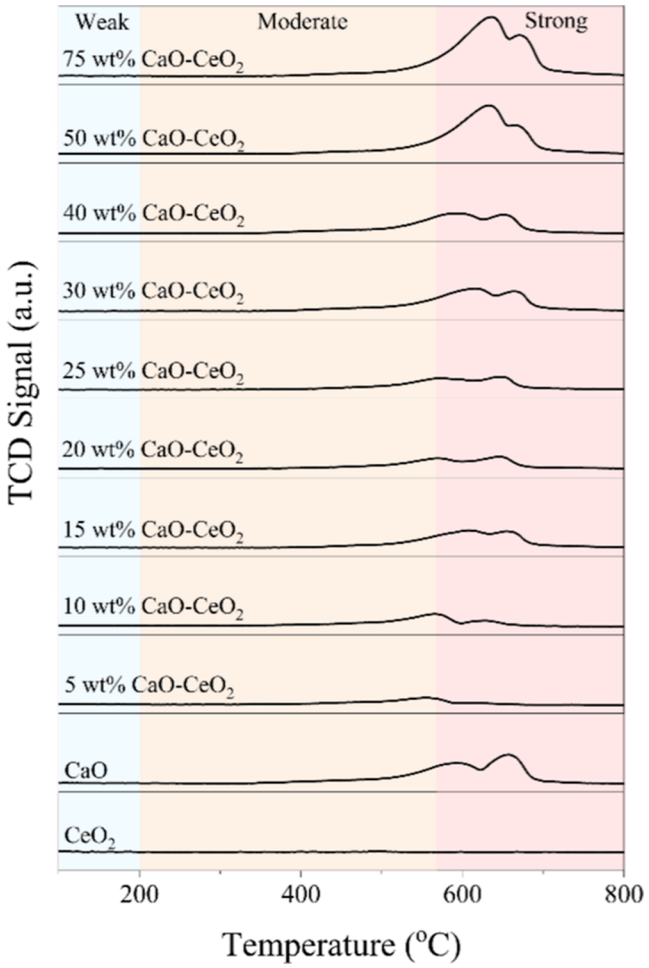

Figure 2. CO_2-TPD profiles of the prepared catalysts.

Figure 3 presents the adsorption−desorption isotherms of the catalysts. The hysteresis loops observed for CeO_2, CaO, and 40 wt % CaO−CeO_2 correspond to type IV hysteresis loops, as classified by the IUPAC, indicating the presence of mesoporous structures.[23]

The TGA results, shown in Figure 4, demonstrate that the CeO_2 catalyst exhibited excellent thermal stability, with no significant weight loss over the evaluated temperature range. In contrast, the CaO catalyst exhibited a notable weight loss of approximately 11% at 400 °C, which was attributed to the decomposition of $Ca(OH)_2$. A second weight loss stage of about 6% was observed between 600 and 700 °C, corresponding to the thermal conversion of $CaCO_3$ to CaO. The 40 wt % CaO−CeO_2 catalyst exhibited a similar two-step weight loss pattern to that of CaO, with a total mass loss of 13%. However, the final residue was higher than that of pure CaO, suggesting that the CeO_2 support enhances the thermal stability of CaO. The weight loss trends observed in the TGA measurements align well with the decomposition behavior of the Ca−Ce oxide catalysts previously reported by Kingkam et al.[23]

Table 2 summarizes the mass percentage calculations based on the metal concentrations (mg kg^{-1}) obtained from ICP analysis. The measured weight percentages of Ca and Ce in the catalysts closely matched the expected theoretical ratio, indicating the successful incorporation of CaO onto the CeO_2 matrix.

The BET surface area, pore volume, and average pore diameter of all catalysts synthesized in this study are summarized in Table 1. The BET surface area is a critical parameter that indicates the available surface area for catalytic activity. CeO_2 showed a BET surface area of 2.46 m^2 g^{-1}, which was higher than that of CaO (1.8 m^2 g^{-1}). However, CaO exhibited a greater pore volume and average pore diameter than pure CeO_2. Following the incorporation of CaO on CeO_2, the BET surface area ranged from 2.00 to 3.25 m^2 g^{-1}, while both the pore volume and average pore diameter increased with CaO doping. The average pore diameter varied between 12.53 and 20.34 nm, which is significantly larger than the molecular diameters of the reactants, glycerol (0.65 nm) and dimethyl carbonate (0.55 nm), while the molecular diameter of the product, glycerol carbonate, is 0.52 nm.[21] Ideally for optimal catalytic performance, the catalyst should possess a pore diameter considerably larger than these molecular dimensions, typically within the mesoporous range (2−50 nm), to facilitate effective diffusion and minimize steric hindrance. However, excessively large pores may reduce the surface area available for catalytic activity.

The morphologies of the catalysts were analyzed using SEM, as shown in Figure 5. Pure CeO_2 exhibited a predominantly spherical structure with a uniform distribution and smaller particle size than CaO (Figure 5a). In contrast, pure CaO appeared as agglomerates of irregularly shaped crystalline particles, as shown in Figure 5b. After mechanical grinding, the particle size of CaO was reduced and became more evenly dispersed on the CeO_2 catalyst. The elemental mapping of the 40 wt % CaO−CeO_2 catalyst (Figure 5f) showed a homogeneous distribution of Ce and Ca oxides, suggesting a possibility of strong interactions between the two metal oxides. When comparing the distribution of Ca and Ce, the mapping revealed a scattered distribution of each element. In Figure 5f, blue specks represent Ca atoms, while yellow specks indicate Ce atoms, showing that Ce is present in significantly higher amounts than Ca. This observation is further supported by the elemental spectrum, which quantifies the weight percentage of each component. The measured Ca−Ce weight percentage ranged from 23% to 78%, aligning well with the expected composition.

3.2. Effect of Different Contents of CaO Doped on CeO_2. To optimize the yield of glycerol carbonate (GC), CeO_2 was doped with varying amounts of calcium oxide (CaO) using a mechanical grinding method. The catalytic performance of the CaO-doped CeO_2 catalysts was evaluated under typical reaction conditions: a catalyst loading of 10 wt %, a reactant molar ratio of 1:3 (GLY: DMC), reaction temperature 90 °C,

https://doi.org/10.1021/acs.energyfuels.5c01580
Energy Fuels XXXX, XXX, XXX−XXX

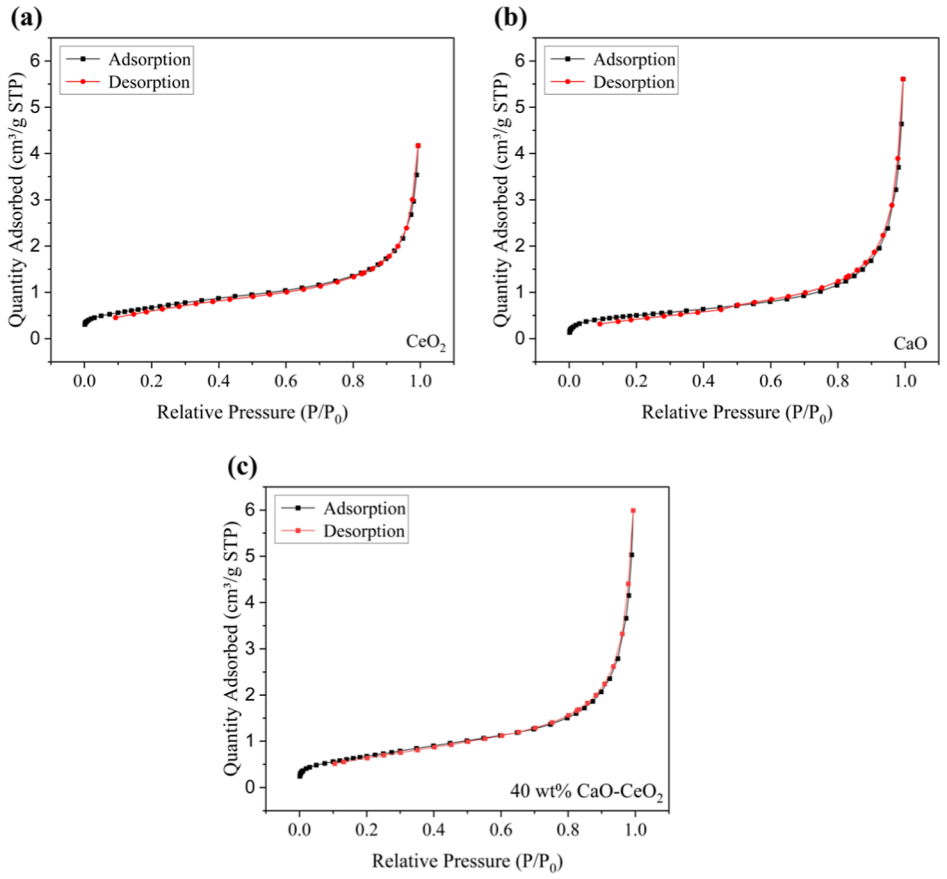

Figure 3. N_2 adsorption/desorption isotherms of CaO−CeO_2 mixed oxide materials: ((a) CeO_2; (b) CaO; and (c) 40 wt % CaO−CeO_2).

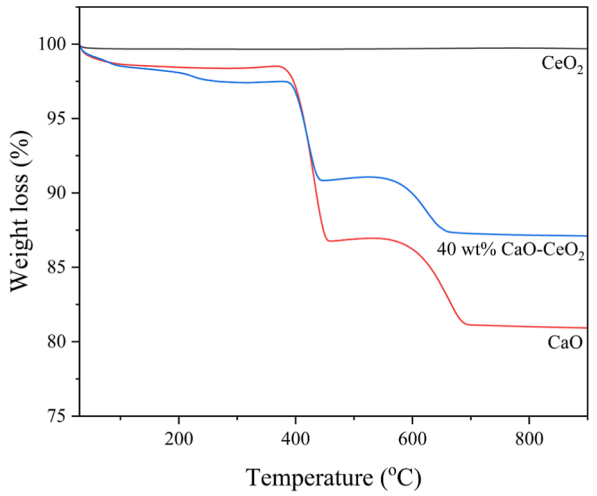

Figure 4. Thermogravimetric analysis (TGA) curves of CeO_2, CaO, and 40 wt % CaO−CeO_2.

Table 2. ICP Analysis of the Prepared Catalysts

catalyst	target CaO content (wt %)	actual CaO content (wt %)	target CeO_2 content (wt %)	actual CeO_2 content (wt %)
5 wt % CaO−CeO_2	5.00	3.74	95.00	96.26
10 wt % CaO−CeO_2	10.00	8.47	90.00	91.53
15 wt % CaO−CeO_2	15.00	12.45	95.00	87.55
20 wt % CaO−CeO_2	20.00	17.02	80.00	82.98
25 wt % CaO−CeO_2	25.00	19.94	75.00	80.06
30 wt % CaO−CeO_2	30.00	27.63	70.00	72.37
40 wt % CaO−CeO_2	40.00	35.35	60.00	65.65
50 wt % CaO−CeO_2	50.00	45.06	50.00	54.94
75 wt % CaO−CeO_2	75.00	71.61	25.00	28.39

and reaction time 1 h. As shown in Figure 6, the highest GC yield of 95% was achieved using 40 wt % CaO doped on CeO_2 as catalyst. The catalytic activity of CeO_2 increased with increasing CaO content, with the GC yield improving progressively from 5 wt % to 40 wt % CaO loading and then similar GC yields for CeO_2 catalysts doped with 50 and 75 wt % CaO. Based on these findings, 40 wt % CaO−CeO_2 was selected for further optimization studies to maximize the GC yield.

3.3. Effect of Catalyst Loading. The transesterification reaction is influenced by the presence of active sites on the basic catalyst, which depends on both the type and amount of metal loading on its surface. A higher number of active sites enhances reactant interactions, thereby improving the conversion efficiency.[28] To determine the optimal catalyst loading for the maximum GC yield, reactions were performed by varying the catalyst loading from 5 to 20 wt % (relative to glycerol). As shown in Figure 7a, the highest GC yield of 94% was achieved using the catalyst loading of 10 wt %. Increasing

https://doi.org/10.1021/acs.energyfuels.5c01580
Energy Fuels XXXX, XXX, XXX−XXX

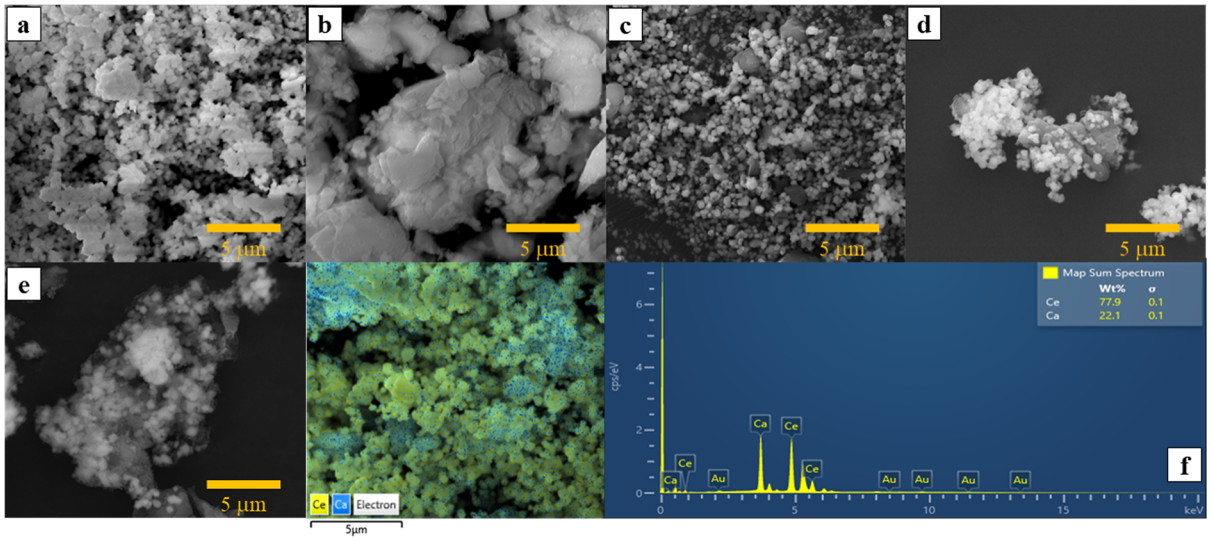

Figure 5. SEM images of (a) CeO_2, (b) CaO catalyst, (c) 40 wt % CaO−CeO_2, (d) used 40 wt % CaO−CeO_2 (calcined at 800 °C), and (e) used 40 wt % CaO−CeO_2 and (f) EDX mapping of 40 wt % CaO−CeO_2.

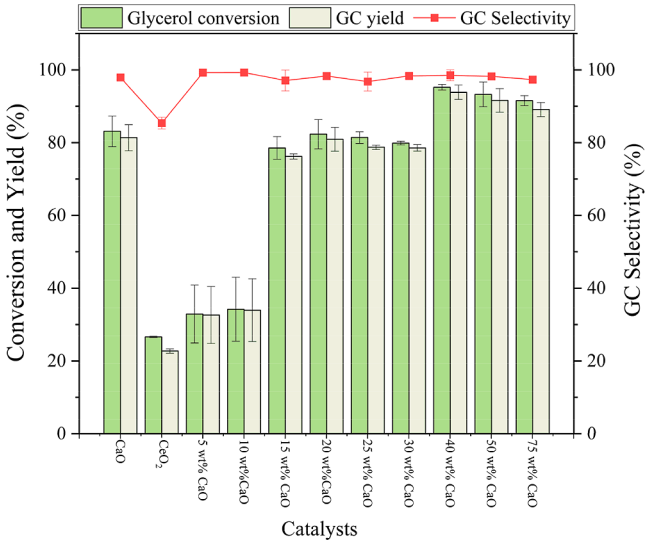

Figure 6. Glycerol conversion, glycerol carbonate selectivity, and yield of prepared CaO, CeO_2, and 5−75 wt % CaO−CeO_2 catalysts.

the catalyst loading beyond 10 wt % did not result in a significant improvement in yield, with a 20 wt % catalyst loading achieving a GC yield of 93%. Therefore, a catalyst loading of 10 wt % was identified as suitable for further parameter optimization in the transesterification reaction.[20,29]

3.4. Effect of Glycerol-to-DMC Mole Ratio. The mole ratio of reactants, glycerol to dimethyl carbonate (GLY:DMC), is a critical factor influencing both the glycerol conversion and the GC yield. In this study, the mole ratio was varied from 1:1 to 1:5 to assess its impact on GC production, as shown in Figure 7b. Initially, increasing the mole ratio of GLY to DMC from 1:1 to 1:3 led to a corresponding increase in the GC yield from 77% to 94%, respectively. Further increase in the mole ratio of GLY to DMC to 1:5 resulted in a decline in the GC yield to 67%. This reduction may be attributed to the increased immiscibility of the reactants. Since glycerol is hydrophilic and DMC is hydrophobic, a higher concentration of DMC in the reaction medium led to phase separation, which hinders mass transfer and reduces the overall reaction efficiency.[29,30]

3.5. Kinetic Model Development. The Weisz−Prater criterion (C_{WP}) was determined to confirm the absence of intraparticle diffusion resistance. This parameter represents the ratio of the intrinsic reaction rate to the intraparticle diffusion rate and serves as an indicator of whether mass transfer limitations affect the reaction kinetics. C_{WP} is determined using

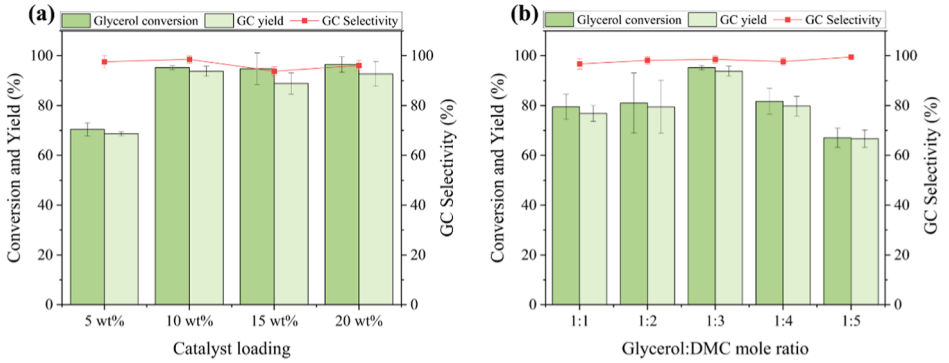

Figure 7. Glycerol conversion, glycerol carbonate selectivity, and yield of 40 wt % CaO−CeO_2 catalyst with (a) different catalyst loadings and (b) different glycerol to DMC mole ratios.

https://doi.org/10.1021/acs.energyfuels.5c01580
Energy Fuels XXXX, XXX, XXX−XXX

the observed reaction rate, particle radius (R_p), effective diffusivity of the limiting reactant (D_e), and the concentration of the reactant at the particle's external surface. The dimensionless Weisz–Prater criterion, C_{WP}, can be calculated by using eq 3 below.

$$C_{WP} = \frac{r_{obs}\rho_c R_p^2}{D_e C_G} \tag{3}$$

where r_{obs} = observed reaction rate (mol kg^{-1} s^{-1}), R_p = catalyst particle radius (m), ρ_c = catalyst density (kg m^{-3}), D_e = effective diffusivity between glycerol and DMC (m^2 s^{-1}), and C_G = bulk liquid glycerol concentration (mol m^{-3}).

The effective diffusivity (D_e) was determined with the following equation

$$D_e = \frac{\varepsilon}{\tau} D_{AB} \tag{4}$$

where ε = porosity of catalyst, τ = tortuosity, and D_{AB} = diffusion coefficient between glycerol and DMC (m^2 s^{-1}) calculated by the Wilke–Chang equation

$$D_{AB} = \frac{7.4 \times 10^{-8} \times (\phi M_A)^{1/2} T}{\eta \times V_B^{0.6}} \tag{5}$$

Finally, r_{obs} is

$$r_{obs} = \frac{N_{A0} - N_{At}}{t} \times \frac{W_c}{\rho_c} \tag{6}$$

where N_{A0} and N_{At} = moles of glycerol at initial and t time (mol), respectively. t = reaction time (s), W_c = mass of catalyst (g).

Conservative estimations for the porosity and tortuosity of the catalyst were 0.05 and 4.41, respectively. The Weisz–Prater Criterion was calculated at different temperatures, as shown in Table 3. The C_{WP} values were much below 1, showing the absence of diffusion limitations and no concentration gradient within the catalyst.

Table 3. Calculated Weisz–Prater Criterion at Different Reaction Temperatures

temperature (°C)	r_{obs} (mol cm^{-3} s^{-1})	D_{AB} (cm^2 s^{-1})	C_{WP}
60	1.105×10^{-6}	2.700×10^{-5}	5.335×10^{-7}
70	1.418×10^{-6}	2.781×10^{-5}	6.651×10^{-7}
80	2.172×10^{-6}	2.862×10^{-5}	9.897×10^{-7}
90	2.592×10^{-6}	2.943×10^{-5}	1.489×10^{-6}

In synthesizing glycerol carbonate, a second-order irreversible kinetic model was developed based on the rate of glycerol conversion. Also, in a prior article, the second-order irreversible kinetic model was developed and validated to describe the effective transesterification of glycerol with DMC.[31] Since the side reaction involving DMC was found to be negligible, only the transesterification of glycerol was considered in the kinetic analysis. Consequently, the kinetic model for glycerol transesterification was simplified to represent the overall reaction, as shown in eq 7.

$$\text{Glycerol} + \text{DMC} \xrightarrow{k} \text{glycerol carbonate} + 2\text{MeOH} \tag{7}$$

The surface reaction of the adsorbed species on the catalyst was assumed to be the rate-determining step. The surface reactions were considered irreversible due to the excess DMC used relative to glycerol. As a result, the kinetic model can be represented by eq 8, where A and B represent glycerol and DMC, respectively.

$$R_A = \frac{dC_A}{dt} = kC_A C_B \tag{8}$$

where k is an irreversible second-order rate constant, C_A is the glycerol concentration, and C_B is the concentration of DMC. According to Teng et al.[31] eq 8 can be written in terms of fractional conversion in the form of eq 9.

$$\frac{dX_A}{dt} = kC_{A0}(1 - X_A)(M - X_A) \tag{9}$$

This, upon integration, leads to

$$\frac{1}{C_{A0}(M-1)} \ln \frac{(M - X_A)}{(1 - X_A)} = kt + C \tag{10}$$

where X_A is the conversion of glycerol. $M = C_{B0}/C_{A0}$, and C_{A0} and C_{B0} are the initial molar concentrations of glycerol and DMC, respectively.

Equation 10 can be written in terms of the linear equation, as below

$$Y(t) = kt + C \tag{11}$$

where

$$Y(t) = \frac{1}{C_{A0}(M-1)} \ln \frac{(M - X_A)}{(1 - X_A)}$$

To validate the reaction kinetics, the irreversible second-order kinetic model was tested by plotting eq 10.

The reaction temperature plays a crucial role in influencing the transesterification process. Typically, as the temperature increases, the reaction rate accelerates, leading to a higher GC yield. To investigate this effect, the reaction temperature was varied between 60 and 90 °C, using a 10 wt % catalyst loading and a GLY to DMC mole ratio of 1:3, with a reaction time of 3 h. A significant increase in both glycerol conversion (Figure 8a) and GC yield (Figure 8b) was observed as the temperature increased from 60 to 90 °C. At 90 °C, a glycerol conversion of 96% was achieved within 1 h, which further increased to 99% after 3 h. A higher reaction temperature increases the frequency of molecular collisions, thereby accelerating the reaction rate. Since the transesterification of DMC with glycerol is an exothermic reaction,[32] increasing the temperature may shift the equilibrium position favorably, resulting in improved glycerol conversion and higher GC yield.[33] Similarly, the GC concentration increased significantly to 4.10 mol L^{-1} at 90 °C, followed by a slight increase to 4.70 mol L^{-1} after 3 h of reaction time.

3.6. Rate Constants and Activation Energy. The conformity of the reaction kinetics with an irreversible second-order kinetic model was evaluated by plotting eq 10 with the results presented in Figure 9. The slope and intercept of the trend lines in the figure correspond to the forward reaction rate constant and the model integration constant, respectively. In addition, the R^2 values of the trend lines indicate the confidence levels of the reaction conformity with the proposed kinetic model. The reaction showed confidence levels in the range of 95–99%, demonstrating a strong agreement with the second-order kinetic model.

The rate constants at different reaction temperatures are summarized in Table 4, determined from the slopes of the

https://doi.org/10.1021/acs.energyfuels.5c01580
Energy Fuels XXXX, XXX, XXX–XXX

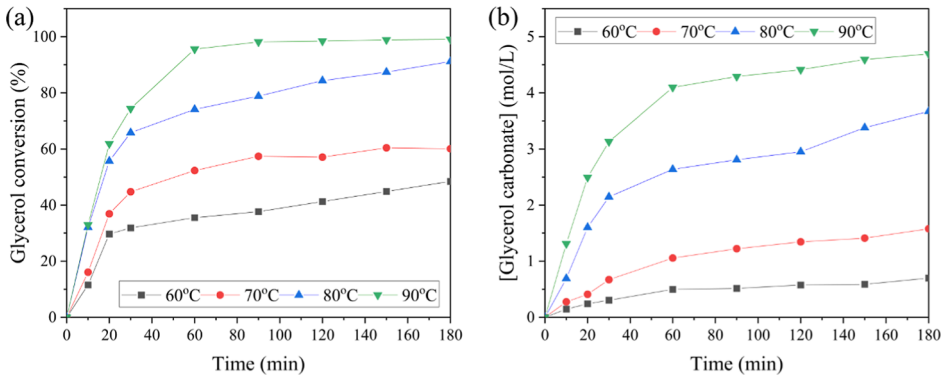

Figure 8. (a) Reaction time profile for glycerol conversion at different temperatures and (b) reaction time profile for glycerol carbonate production at different temperatures.

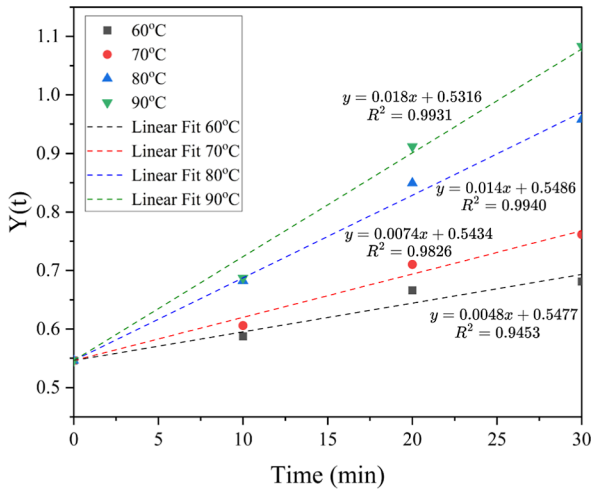

Figure 9. Plot of $Y(t)$ against time at a different temperature is achieved from the irreversible second-order kinetic model.

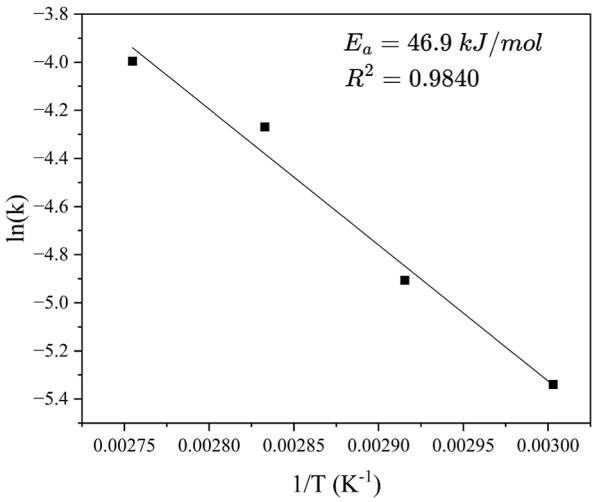

Figure 10. Arrhenius plot for the irreversible second-order kinetic model for the transesterification of glycerol with DMC.

Table 4. Rate Constants for the Transesterification

temperature (°C)	rate constant, k (L mol^{-1} s^{-1})
60	0.0048
70	0.0074
80	0.0140
90	0.0180

trendlines presented in Figure 9 and calculated using eq 4. The lowest rate constant, 0.0048 L mol^{-1} min^{-1}, was obtained at 60 °C, while the highest, 0.0180 L mol^{-1} min^{-1}, was observed at 90 °C. This indicated that increasing the temperature enhances the reaction rate, thereby reducing the time required to achieve a maximum product yield. These findings align with previously discussed equilibrium times at various temperatures. The activation energy of the reaction was calculated using the Arrhenius equation, as shown in eq 12. The data in Table 4 clearly demonstrate that the apparent reaction rate constant increases with temperature from 60 to 90 °C, indicating that equilibrium is reached more rapidly at higher temperatures. The activation energy for the transesterification reaction, calculated from the Arrhenius plot in Figure 10, was found to be 46.9 kJ mol^{-1}. Literature values for activation energy for this reaction typically range between 28.4 and 52.5 kJ mol^{-1}.[32,34−36] These results confirm that the reaction proceeded without mass transfer limitations.

$$k = A\ \mathrm{Exp}\left(-\frac{E_a}{RT}\right) \tag{12}$$

where E_a is the activation energy and A is the frequency factor. In the plot of ln k versus $1/T$, the slope and the intercept of the trend line denote the value of E_a/R and A, respectively.

3.7. Catalyst Reusability. The consecutive reaction cycles were performed to evaluate the stability and reusability of the catalysts with the results shown in Figure 11. The catalyst showed sustained activity, maintaining high glycerol conversion and GC yield over four reaction cycles. The spent catalysts were characterized using XRD and FTIR spectroscopy to evaluate the structural changes in the surface CaO species. As shown in Figure 12a, XRD patterns of the used 40 wt % CaO−CeO_2 revealed peaks corresponding to $CaCO_3$ at 17° and $Ca(OH)_2$ at 35° and 52°. Also, some CaO peaks present in the fresh catalyst were absent in the used catalyst. According to Praikaew et al.,[21] transformation of CaO can occur via the formation of $Ca(OH)_2$ and $CaCO_3$ species during the reaction process. The formation of $CaCO_3$ may be influenced by an excess of DMC relative to glycerol, potentially facilitating a condensation reaction between glycerol and CaO. This leads to the in situ generation of water and water-derived species. Consequently, CaO can undergo further reaction with DMC and water, producing methanol and $CaCO_3$. Moreover, SEM analysis (Figure 5e) indicated that the $CaCO_3$ formed

https://doi.org/10.1021/acs.energyfuels.5c01580
Energy Fuels XXXX, XXX, XXX−XXX

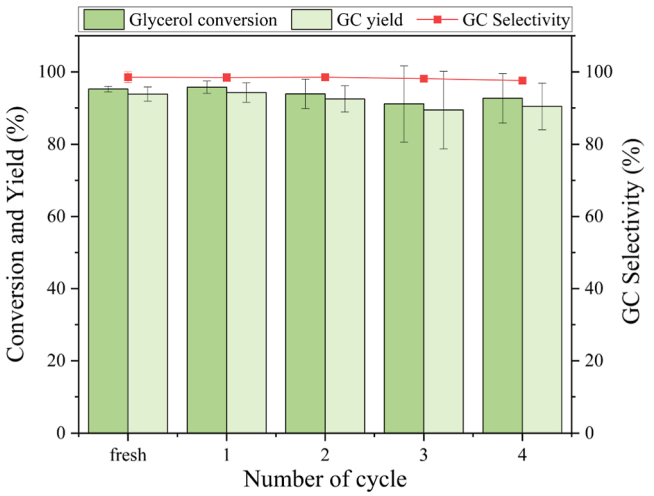

Figure 11. Effect of 40 wt % $CaO-CeO_2$ reusability on glycerol conversion and product yield.

during the reaction existed as an amorphous layer on the catalyst surface, altering its morphology to smoother, rounded, and irregularly shaped particles.[20] When the used catalyst was recovered and calcined at 800 °C for 3 h, it converted $CaCO_3$ and $Ca(OH)_2$ back into CaO. The XRD patterns of the used catalyst calcined at 800 °C were similar to those of the fresh catalyst, confirming the regeneration of CaO. FTIR analysis (Figure 12b) further validated this transformation. After the reaction, a peak at 875 cm^{-1} became sharper compared to the fresh and calcined catalysts, which can be attributed to the out-of-plane stretching vibrations of the carbonate group (CO_3). Additionally, the band at 1397 cm^{-1} exhibited an increased intensity after the reaction, corresponding to the asymmetric stretching of the C−O bond in the carbonate group. Additional bands at approximately 1489 cm^{-1} appeared, which could be associated with C−O stretching in esters or alcohols and alkyl group stretching, respectively. Notably, the band at 1043 cm^{-1} is characteristic to C−O stretching vibrations in the methoxide ($-OCH_3$) group of calcium methoxide, indicating that CaO initially reacts with methanol to form calcium methoxide, which then hydrolyzes to $Ca(OH)_2$ and subsequently might convert to $CaCO_3$ upon exposure to moisture and CO_2.[21] These findings confirm that calcination effectively removes surface impurities and facilitates the regeneration of CaO, thereby maintaining catalytic activity and glycerol conversion efficiency.

3.8. Catalyst Stability. The leaching test was performed to investigate the catalyst stability by the hot filtration method. After 30 min of reaction, the catalyst was removed from the reaction mixture by filtration, and the resulting filtrate was continued without catalyst under the same reaction conditions for an additional 60 min. As illustrated in Figure 13a, no further conversion of glycerol was observed following the removal of the 40 wt % $CaO-CeO_2$ catalyst. This result indicates that the catalyst remains largely heterogeneous during the reaction, suggesting minimal leaching. The presence of CeO_2 enhanced the structural integrity of the catalyst, acting as a stabilizing support and inhibiting the dissolution of the active CaO species. In contrast, when pure CaO was employed as the catalyst, the reaction continued gradually even after its removal, achieving 70% glycerol conversion at 90 min of reaction time—comparable to that achieved with the catalyst present throughout the reaction period (Figure 13b). This observation implies partial leaching of the active species from the pure CaO catalyst into the reaction medium.

3.9. Reaction Mechanism. A plausible reaction mechanism for the transesterification of glycerol with dimethyl carbonate (DMC) over heterogeneous base catalysts, including CaO and Ca-doped metal oxides, has been widely investigated in previous studies.[11,20,21,28,33,37] Herein, we propose the mechanism for glycerol carbonate formation on the surface of

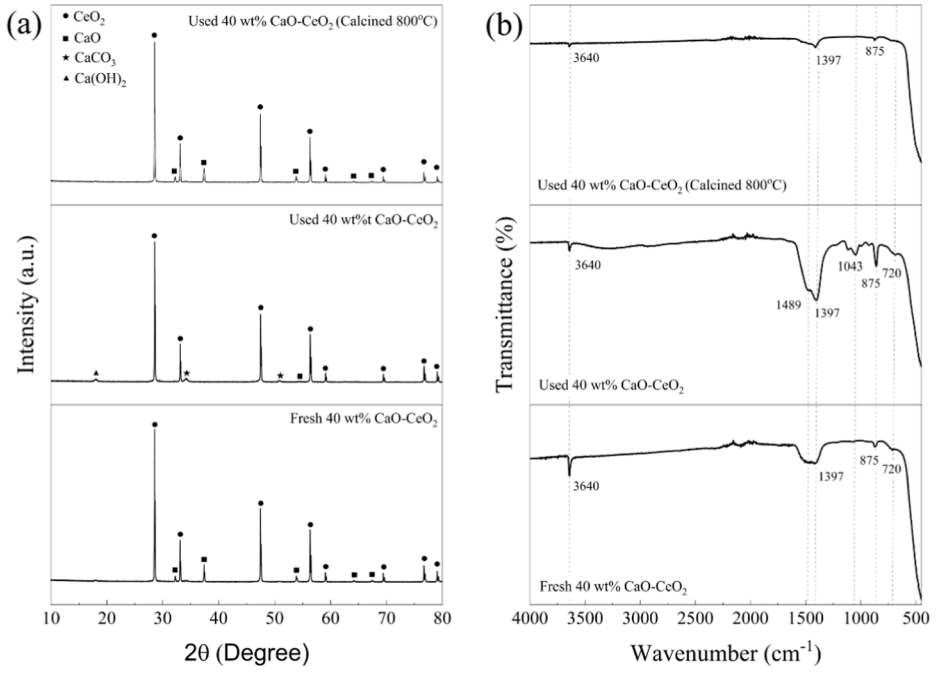

Figure 12. (a) X-ray diffraction patterns of used 40 wt % $CaO-CeO_2$ catalysts before and after calcination, and (b) FTIR spectra of used 40 wt % $CaO-CeO_2$ catalysts before and after calcination.

https://doi.org/10.1021/acs.energyfuels.5c01580
Energy Fuels XXXX, XXX, XXX−XXX

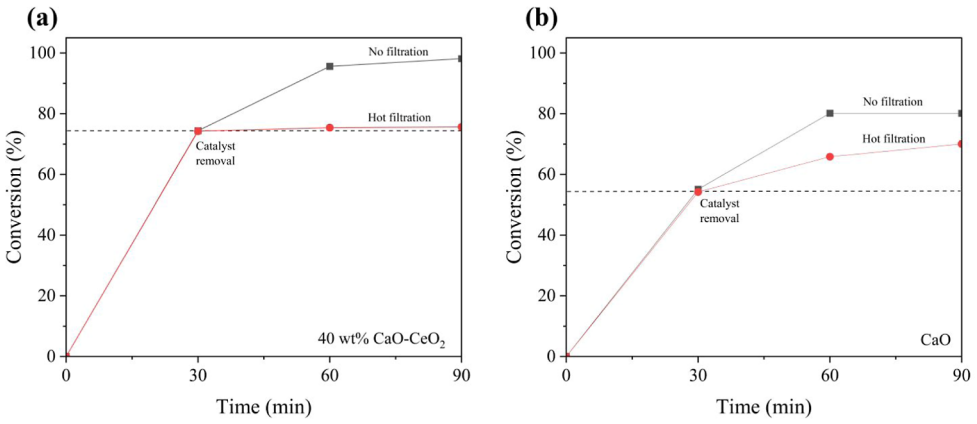

Figure 13. Hot filtration method for the evaluation of catalyst leaching: (a) 40 wt % $CaO-CeO_2$ catalysts and (b) CaO catalyst.

Scheme 1. Plausible Mechanism of Transesterification between Glycerol with DMC over $CaO-CeO_2$ Catalyst

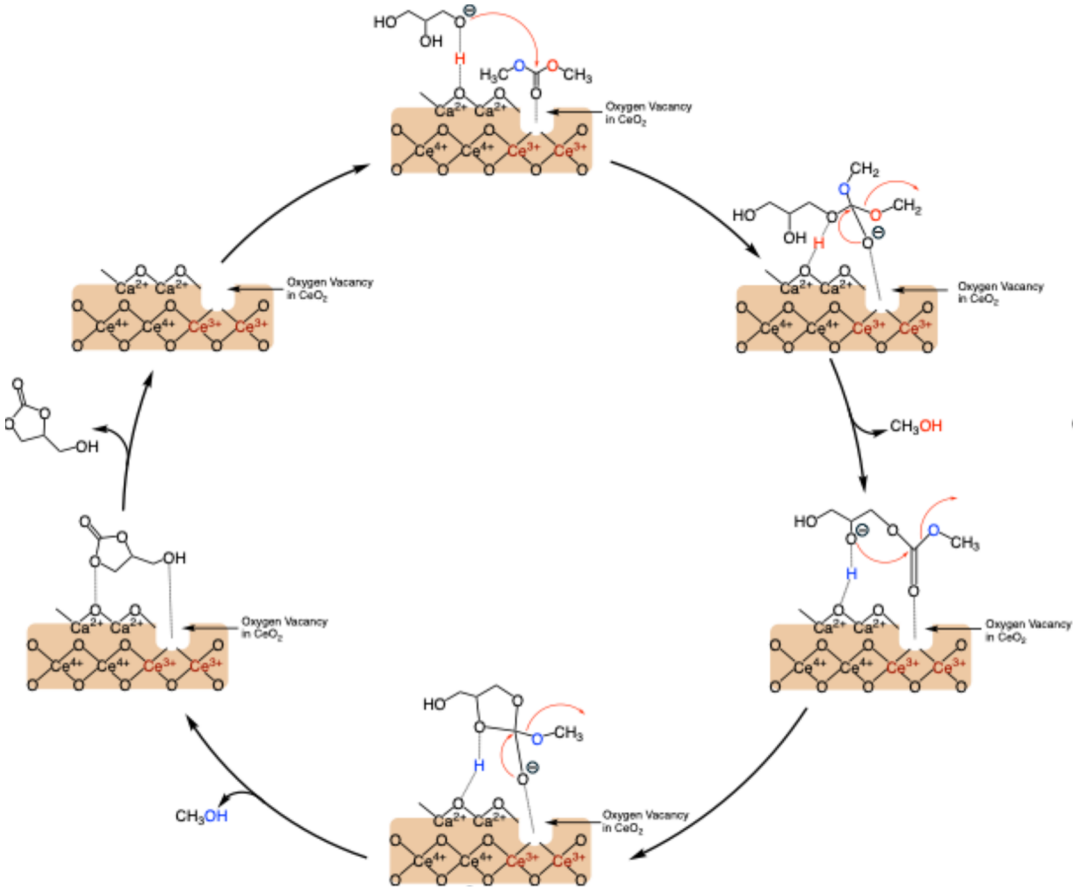

the $CaO-CeO_2$ catalyst via synergistic interaction, as illustrated in Scheme 1. Catalyst characterization, particularly CO_2-TPD along with catalytic activity tests, indicate that the total basicity of $CaO-CeO_2$ mixed oxides increases with CaO doping, correlating with a higher GC yield. Scheme 1 highlights the synergistic interaction between basic active sites of the O^{2-} anions, $Ca^{2+}-O^{2-}$ pairs, and oxygen vacancies in the CeO_2 matrix at the $CaO-CeO_2$ interface. Initially, glycerol adsorbs onto the basic active sites of the catalyst, specifically, the O^{2-} anions and $Ca^{2+}-O^{2-}$ pairs, while the carbonyl group of DMC interacts with oxygen vacancies in CeO_2. The basic sites of O^{2-} and $Ca^{2+}-O^{2-}$ activate glycerol, forming a glyceroxide anion via hydrogen bonding. Simultaneously, the electron-rich carbonyl oxygen in DMC interacts with Ce^{3+} sites at the oxygen vacancies. The glyceroxide anion at the $CaO-CeO_2$ interface then nucleophilically attacks the carbonyl group of DMC adsorbed on Ce^{3+} sites, forming a methyl glyceryl carbonate intermediate and releasing a methoxide anion, which subsequently converts into methanol. In the final step, an adjacent hydroxyl group's activated oxygen attacks the carbonyl carbon, facilitating cyclization and yielding glycerol carbonate, with methanol as a byproduct.

3.10. Activity Comparison. The catalytic performance of the 40 wt % $CaO-CeO_2$ catalyst was compared with that of various heterogeneous catalysts previously reported for the transesterification of glycerol with dimethyl carbonate (DMC),

https://doi.org/10.1021/acs.energyfuels.5c01580
Energy Fuels XXXX, XXX, XXX−XXX

Table 5. Comparison of 40 wt % $CaO-CeO_2$ Catalyst with Other Reported Catalysts for the Synthesis of Glycerol Carbonate

catalyst	temperature (°C)	catalyst dosage (wt %)	DMC/Gly	time (min)	GC yield (%)	ref
CaO	95	5%	5	120	70.0	38
0.5 Ben/CaO	95	5%	5	120	82.0	38
15 wt % Na_2CO_3−Cs-800	75	3%	5	90	96.0	20
5 wt % Co/MCM-41	90	6%	3	120	94.1	36
MMO-$Cu_{15}Zn_{15}$	85	7.5%	2	270	85.1	44
Mg/ZnO	80	3%	4	120	96.5	41
6MgO/g-C_3N_4	80	5%	3	240	97.1	39
Mg_3Ce_1	90	15%	5	90	86.0	15
$Mg_{2.4}Al_{1.0}Cu_{0.6}$	90	15%	5	90	91.2	45
$Mg_3Al_1Zr_1$	75	10%	5	90	94.0	43
1:2 CuO/ZnO/MnO_2	90	3%	5	90	97.0	42
$CoFe_2O_4$/CaO−ZnO	85	5%	5	150	97.7	40
40 wt % $CaO-CeO_2$	90	10%	3	90	98.1	in this work

as summarized in Table 5. Under optimized conditions (90 °C, 10 wt % catalyst loading, DMC/glycerol molar ratio of 3, and 90 min of reaction time), the $CaO-CeO_2$ catalyst achieved an outstanding glycerol carbonate (GC) yield of 98%. This yield exceeds those reported for conventional CaO (70%)[38] and modified CaO systems such as 0.5 Ben/CaO (82%)[38] under similar conditions, requiring longer reaction times and delivering significantly lower conversions.

Other catalysts have demonstrated competitive yields, although with compromises in reaction time, temperature, and catalyst complexity. For example, 6MgO/g-C_3N_4 and $CoFe_2O_4$/CaO−ZnO achieved yields of 97% and 98%, respectively, but required prolonged reaction times of 240 and 150 min[39,40] Likewise, Mg/ZnO and Na_2CO_3−Cs-800 catalysts yielded 97% and 96%, respectively, yet required longer durations or specific synthetic modifications.[20,41] Notably, multicomponent systems such as 1:2 CuO/ZnO/MnO_2 (97%) and Mg_3AlZr_1 (94%) also exhibited high performance, however, involving more complex formulations that may limit their scalability.[42,43]

Conversely, the $CaO-CeO_2$ catalyst provides an advantageous combination of high activity, short reaction time, and operational simplicity. Moreover, its preparation via a green, solvent-free method and using earth-abundant components are economically and environmentally sustainable options for industrial implementation in glycerol carbonate production.

4. CONCLUSION

A sustainable approach for synthesizing glycerol carbonate from glycerol and dimethyl carbonate was demonstrated using a supported CaO catalyst. Cerium oxide (CeO_2) served as a support material, enhancing the catalyst stability and activity. Among the catalyst compositions tested, 40 wt % $CaO-CeO_2$ exhibited the highest catalytic performance, achieving a glycerol carbonate yield exceeding 95% at 90 °C. The catalyst showed excellent stability and reusability, maintaining its high performance over four cycles. A comprehensive kinetic model was developed based on irreversible second-order kinetics. The activation energy for the transesterification reaction, determined from an Arrhenius plot, was calculated as 46.9 kJ mol^{-1}, confirming that the reaction proceeded within the kinetic regime rather than being diffusion-limited. Overall, this study highlights the effectiveness of mechanochemically prepared $CaO-CeO_2$ catalysts in enabling the green synthesis of glycerol carbonate, offering a promising route for a sustainable circular economic process.

AUTHOR INFORMATION

Corresponding Author

Haresh Manyar − *School of Chemistry and Chemical Engineering, Queen's University Belfast, Belfast BT9 5AG, U.K.*; orcid.org/0000-0002-7990-4410; Email: h.manyar@qub.ac.uk

Authors

Patcharaporn Inrirai − *School of Chemistry and Chemical Engineering, Queen's University Belfast, Belfast BT9 5AG, U.K.*

Runzhe Yu − *School of Chemistry and Chemical Engineering, Queen's University Belfast, Belfast BT9 5AG, U.K.*

Daniel Goma Jiménez − *School of Chemistry and Chemical Engineering, Queen's University Belfast, Belfast BT9 5AG, U.K.*; orcid.org/0000-0002-9950-0122

Nancy Artioli − *Department of Civil, Environmental, Architectural Engineering and Mathematics, University of Brescia, Brescia 25123, Italy*

Complete contact information is available at: https://pubs.acs.org/10.1021/acs.energyfuels.5c01580

Author Contributions

The manuscript was written through contributions of all authors. All authors have given approval to the final version of the manuscript.

Notes

The authors declare no competing financial interest.

ACKNOWLEDGMENTS

The authors gratefully acknowledge the financial support for PhD scholarship to P.I. funded by the Royal Thai government. H.M. thankfully acknowledges the funding and support provided by the Leverhulme Trust research grant RPG-2020-301 as well as the UK Catalysis hub via our membership of the UK Catalysis Hub Consortium funded by EPSRC grant: EP/R026645/1.

ABBREVIATIONS

DMC: dimethyl carbonate; Eqn: equation; GC: glycerol carbonate; GLY: glycerol

REFERENCES

(1) Abdelrahman, A. A.; Abo El-Khair, M. A. Advanced Biodiesel Production: Feedstocks, Technologies, Catalysts, Challenges, and Environmental Impacts. *J. Environ. Chem. Eng.* **2025**, *13* (1), 114966.

https://doi.org/10.1021/acs.energyfuels.5c01580
Energy Fuels XXXX, XXX, XXX−XXX

(2) Attarbachi, T.; Kingsley, M. D.; Spallina, V. New trends on crude glycerol purification: A review. *Fuel* **2023**, *340*, 127485.
(3) Nguyen, R.; Halloumi, S.; Malpartida, I.; Len, C. Solvent-Free Production of Triacetin from Glycerol through Complementary Mechanochemical, Biphasic, and Catalytic Approaches Using ICHeM Technology. *Org. Process Res. Dev.* **2025**, *29* (3), 769−777.
(4) Keogh, J.; Deshmukh, G.; Manyar, H. Green synthesis of glycerol carbonate via transesterification of glycerol using mechanochemically prepared sodium aluminate catalysts. *Fuel* **2022**, *310*, 122484.
(5) Keogh, J.; Jeffrey, C.; Tiwari, M. S.; Manyar, H. Kinetic Analysis of Glycerol Esterification Using Tin Exchanged Tungstophosphoric Acid on K-10. *Ind. Eng. Chem. Res.* **2022**, *62* (45), 19095−19103.
(6) Pandit, K.; Jeffrey, C.; Keogh, J.; Tiwari, M. S.; Artioli, N.; Manyar, H. G. Techno-Economic Assessment and Sensitivity Analysis of Glycerol Valorization to Biofuel Additives via Esterification. *Ind. Eng. Chem. Res.* **2023**, *62* (23), 9201−9210.
(7) Keogh, J.; Inrirai, P.; Artioli, N.; Manyar, H. Nanostructured Solid/Liquid Acid Catalysts for Glycerol Esterification: The Key to Convert Liability into Assets. *Nanomaterials* **2024**, *14* (7), 615.
(8) Inrirai, P.; Keogh, J.; Centeno-Pedrazo, A.; Artioli, N.; Manyar, H. Recent advances in processes and catalysts for glycerol carbonate production via direct and indirect use of CO_2. *J. CO2 Util.* **2024**, *80*, 102693.
(9) Gosu, V.; Arora, S.; Subbaramaiah, V.; Srivastava, V. C.; Gupta, R. B. Glycerol Carbonate Synthesis: Critical Analysis of Prospects and Challenges with Special Emphasis on Influencing Parameters for Catalytic Transesterification. *ACS Sustainable Resour. Manage.* **2024**, *1* (5), 816−841.
(10) Ochoa-Gómez, J. R.; Gómez-Jiménez-Aberasturi, O.; Maestro-Madurga, B.; Pesquera-Rodríguez, A.; Ramírez-López, C.; Lorenzo-Ibarreta, L.; Torrecilla-Soria, J.; Villarán-Velasco, M. C. Synthesis of glycerol carbonate from glycerol and dimethyl carbonate by transesterification: Catalyst screening and reaction optimization. *Appl. Catal., A* **2009**, *366* (2), 315−324.
(11) Simanjuntak, F. S. H.; Kim, T. K.; Lee, S. D.; Ahn, B. S.; Kim, H. S.; Lee, H. CaO-catalyzed synthesis of glycerol carbonate from glycerol and dimethyl carbonate: Isolation and characterization of an active Ca species. *Appl. Catal., A* **2011**, *401* (1), 220−225.
(12) Lu, P.; Wang, H.; Hu, K. Synthesis of glycerol carbonate from glycerol and dimethyl carbonate over the extruded CaO-based catalyst. *Chem. Eng. J.* **2013**, *228*, 147−154.
(13) Hu, K.; Wang, H.; Liu, Y.; Yang, C. KNO_3/CaO as cost-effective heterogeneous catalyst for the synthesis of glycerol carbonate from glycerol and dimethyl carbonate. *J. Ind. Eng. Chem.* **2015**, *28*, 334−343.
(14) Wu, Y.; Song, X.; Zhang, J.; Li, S.; Yang, X.; Wang, H.; Wei, R.; Gao, L.; Zhang, J.; Xiao, G. Synthesis of glycerol carbonate from glycerol and diethyl carbonate over CeO_2-CdO catalyst: The role of Ce^{4+} doped into CdO lattice. *J. Taiwan Inst. Chem. Eng.* **2018**, *87*, 131−139.
(15) Parameswaram, G.; Rao, P. S. N.; Srivani, A.; Rao, G. N.; Lingaiah, N. Magnesia-ceria mixed oxide catalysts for the selective transesterification of glycerol to glycerol carbonate. *Mol. Catal.* **2018**, *451*, 135−142.
(16) Niu, S.; Zhang, X.; Ning, Y.; Zhang, Y.; Qu, T.; Hu, X.; Gong, Z.; Lu, C. Dolomite incorporated with cerium to enhance the stability in catalyzing transesterification for biodiesel production. *Renewable Energy* **2020**, *154*, 107−116.
(17) Arora, S.; Gosu, V.; Kumar, U. K. A.; Zhang, T. C.; Subbaramaiah, V. A novel Ce-CaO/MgO catalyst derived from marble waste through green synthesis route for glycerol carbonate synthesis. *React. Kinet., Mech. Catal.* **2021**, *132* (2), 839−858.
(18) Kong, J.; Xiang, Z.; Li, G.; An, T. Introduce oxygen vacancies into CeO_2 catalyst for enhanced coke resistance during photo-thermocatalytic oxidation of typical VOCs. *Appl. Catal., B* **2020**, *269*, 118755.
(19) Li, Y.; Wu, J.; Liu, F.; Liu, W.; Li, B.; Zhang, Q.; Wang, M.; Yang, H.; Fang, Z.; Ma, Z. Promotion mechanism of rare-earth elements doping on performance of CaO/CeO_2 sorbent for high temperature CO_2 capture. *Chem. Eng. J.* **2025**, *507*, 160675.
(20) Wang, J.; Wang, Z.; Liu, H.; Wang, S.; Sun, Y. Synthesis of Glycerol Carbonate from Glycerol and Dimethyl Carbonate Catalyzed by Solid Base Catalyst Derived from Waste Carbide Slag. *Int. J. Polym. Sci.* **2021**, *2021* (1), 1−14.
(21) Praikaew, W.; Kiatkittipong, W.; Aiouache, F.; Najdanovic-Visak, V.; Termtanun, M.; Lim, J. W.; Lam, S. S.; Kiatkittipong, K.; Laosiripojana, N.; Boonyasuwat, S.; et al. Mechanism of CaO catalyst deactivation with unconventional monitoring method for glycerol carbonate production via transesterification of glycerol with dimethyl carbonate. *Int. J. Energy Res.* **2022**, *46* (2), 1646−1658.
(22) Pradhan, G.; Sharma, Y. C. A greener and cheaper approach towards synthesis of glycerol carbonate from bio waste glycerol using CaO−TiO_2 Nanocatalysts. *J. Cleaner Prod.* **2021**, *315*, 127860.
(23) Kingkam, W.; Maisomboon, J.; Khamenkit, K.; Nuchdang, S.; Nilgumhang, K.; Issarapanacheewin, S.; Rattanaphra, D. Preparation of CaO@CeO_2 Solid Base Catalysts Used for Biodiesel Production. *Catalysts* **2024**, *14* (4), 240.
(24) Teo, S. H.; Rashid, U.; Taufiq-Yap, Y. H. Heterogeneous catalysis of transesterification of jatropha curcas oil over calcium−cerium bimetallic oxide catalyst. *RSC Adv.* **2014**, *4* (90), 48836−48847.
(25) de Paula, G. M.; Eid, J. G.; de Paula, L. d. N. R.; Cardoso, D. Understanding the reaction dynamics of glycerol conversion into glycerol carbonate by transesterification of carbonic acid esters over CaO. *Catal. Today* **2024**, *442*, 114953.
(26) Zhang, N.; Xue, H.; Hu, R. The activity and stability of CeO(2)@CaO catalysts for the production of biodiesel. *RSC Adv.* **2018**, *8* (57), 32922−32929.
(27) Podila, S.; Al-Zahrani, A. A.; Pasupulety, N.; Alamoudi, M. A. Influence of CaCe ratio on the hydrogen production from ammonia over CaO-CeO_2 supported Co catalysts. *Arabian J. Chem.* **2023**, *16* (11), 105235.
(28) Kondawar, S. E.; Patil, C. R.; Rode, C. V. Tandem Synthesis of Glycidol via Transesterification of Glycerol with DMC over Ba-Mixed Metal Oxide Catalysts. *ACS Sustainable Chem. Eng.* **2017**, *5* (2), 1763−1774.
(29) Gautam, P.; Barman, S.; Ali, A. Synthesis of glycerol carbonate using Li/Mg/K modified zeolite beta: a kinetic study. *New J. Chem.* **2024**, *48* (10), 4617−4628.
(30) Chotchuang, A.; Kunsuk, P.; Phanpitakkul, A.; Chanklang, S.; Chareonpanich, M.; Seubsai, A. Production of glycerol carbonate from glycerol over modified sodium-aluminate-doped calcium oxide catalysts. *Catal. Today* **2022**, *388−389*, 351−359.
(31) Teng, W. K.; Yusoff, R.; Aroua, M. K.; Ngoh, G. C. Process optimization and kinetics of microwave assisted transesterification of crude glycerol for the production of glycerol carbonate. *Sustainable Energy Fuels* **2021**, *5* (1), 274−282.
(32) Esteban, J.; Domínguez, E.; Ladero, M.; Garcia-Ochoa, F. Kinetics of the production of glycerol carbonate by transesterification of glycerol with dimethyl and ethylene carbonate using potassium methoxide, a highly active catalyst. *Fuel Process. Technol.* **2015**, *138*, 243−251.
(33) Zhu, J.; Chen, D.; Wang, Z.; Wu, Q.; Yin, Z.; Wei, Z. Synthesis of glycerol carbonate from glycerol and dimethyl carbonate over CaO-SBA-15 catalyst. *Chem. Eng. Sci.* **2022**, *258*, 117760.
(34) Yadav, G. D.; Chandan, P. A. A green process for glycerol valorization to glycerol carbonate over heterogeneous hydrotalcite catalyst. *Catal. Today* **2014**, *237*, 47−53.
(35) Qing, Y.; Lu, H.; Liu, Y.; Liu, C.; Liang, B.; Jiang, W. Production of glycerol carbonate using crude glycerol from biodiesel production with DBU as a catalyst. *Chin. J. Chem. Eng.* **2018**, *26* (9), 1912−1919.
(36) Arora, S.; Gosu, V.; Subbaramaiah, V.; Zhang, T. C. Catalytic transesterification of glycerol with dimethyl carbonate to glycerol carbonate with CoO nanoparticle incorporated MCM-41 derived from rice husk. *Can. J. Chem. Eng.* **2022**, *100* (8), 1868−1883.

https://doi.org/10.1021/acs.energyfuels.5c01580
Energy Fuels XXXX, XXX, XXX−XXX

(37) Zhang, X.; Wei, S.; Zhao, X.; Chen, Z.; Wu, H.; Rong, P.; Sun, Y.; Li, Y.; Yu, H.; Wang, D. Preparation of mesoporous CaO-ZrO_2 catalysts without template for the continuous synthesis of glycerol carbonate in a fixed-bed reactor. *Appl. Catal., A* **2020**, *590*, 117313.
(38) Kaur, A.; Ali, A. Surface-Modified CaO Catalyst for the Production of Glycerol Carbonate. *ChemistrySelect* **2021**, *6* (24), 6102−6114.
(39) Reisi, B.; Najafi Chermahini, A. Modification g-C_3N_4 by MgO and its application for glycerol carbonate synthesis from glycerol and dimethyl carbonate. *Environ. Prog. Sustainable Energy* **2023**, *42* (2), No. e14007.
(40) Zhang, P.; Chen, Y.; Zhu, M.; Yue, C.; Dong, Y.; Leng, Y.; Fan, M.; Jiang, P. Acidic−Basic Bifunctional Magnetic Mesoporous $CoFe_2O_4$@(CaO−ZnO) for the Synthesis of Glycerol Carbonate. *Catal. Lett.* **2020**, *150* (10), 2863−2872.
(41) Pradhan, G.; Sharma, Y. C. Green synthesis of glycerol carbonate by transesterification of bio glycerol with dimethyl carbonate over Mg/ZnO: A highly efficient heterogeneous catalyst. *Fuel* **2021**, *284*, 118966.
(42) Lian, J.; Zhang, L.; Xia, L.; Wang, L.; Zhou, X.; Lin, S.; Vinogradov, J.; Lu, J. Highly efficient synthesis of glycerol carbonate over CuO/ZnO/MnO_2 catalyst. *Mater. Today Chem.* **2025**, *43*, 102523.
(43) Malyaadri, M.; Jagadeeswaraiah, K.; Sai Prasad, P. S.; Lingaiah, N. Synthesis of glycerol carbonate by transesterification of glycerol with dimethyl carbonate over Mg/Al/Zr catalysts. *Appl. Catal., A* **2011**, *401* (1), 153−157.
(44) Argüello, D. S.; Cabana Saavedra, L. C.; Mendoza, S. M.; Oliva, M. I.; Rodríguez-Castellón, E.; Bálsamo, N. F.; Eimer, G. A.; Crivello, M. E. Layered double hydroxides modified by transition metals for sustainable glycerol valorization to glycerol carbonate. *Catal. Today* **2024**, *427*, 114415.
(45) Marimuthu, M.; Marimuthu, P.; S. K, S.; Palanivelu, S.; Rajagopalan, V. Tuning the basicity of Cu-based mixed oxide catalysts towards the efficient conversion of glycerol to glycerol carbonate. *Mol. Catal.* **2018**, *460*, 53−62.

https://doi.org/10.1021/acs.energyfuels.5c01580
Energy Fuels XXXX, XXX, XXX−XXX